Experiments in Fluids manuscript No.
(will be inserted by the editor)

A. J. Saddington · R. D. Knowles · K. Knowles

LDA Measurements in the Near-Wake of an Isolated Formula One Wheel

Received: / Accepted:

Abstract An experimental investigation was conducted to identify the main structures in the near wake of an isolated Formula One wheel rotating in ground contact. A 50 per cent-scale isolated wheel assembly, geometrically similar to the configuration mounted on a Formula One racing car, was tested in a closed-return

A. J. Saddington

Department of Aerospace, Power and Sensors, Cranfield University, Defence Academy of the United Kingdom, Shrivenham, Swindon, SN6 8LA, UK

Tel: +44 1793 785219

E-mail: a.j.saddington@cranfield.ac.uk

R. D. Knowles

Department of Aerospace, Power and Sensors, Cranfield University, Defence Academy of the United Kingdom, Shrivenham, Swindon, SN6 8LA, UK

Present address: Advantage CFD, Reynard Park, Brackley, Northamptonshire, NN13 7RP, UK

K. Knowles

Department of Aerospace, Power and Sensors, Cranfield University, Defence Academy of the United Kingdom, Shrivenham, Swindon, SN6 8LA, UK

three-quarter open-jet wind tunnel. The test Reynolds number, based on wheel diameter was $6.8 \cdot 10^5$. Using laser doppler anemometry, three velocity components were measured with a total of 1 966 data points across four planes and within one diameter downstream of the wheel axis. Based on analysis of these data, the main characteristics of the near-wake of an isolated wheel rotating in ground contact are presented. A revised model of the trailing vortex system induced in the wake of such a wheel is proposed, which clarifies the contradictory ones published in the literature to date.

Keywords LDA · F1 · wheel · wake

Symbols

D wheel diameter

f focal length (of laser doppler anemometer probe)

t transit time (of seeding particle)

u velocity component in the x-direction

u_∞ freestream velocity

v velocity component in the y-direction

w velocity component in the z-direction

x streamwise Cartesian coordinate (see Figure 3)

y crosswise Cartesian coordinate (see Figure 3)

z vertical Cartesian coordinate (see Figure 3)

τ_i integral timescale

1 Introduction

The exposed wheels of monoposto (single-seat) racing cars, such as Formula One cars, are tightly regulated to ensure that the formulae retain their distinctive appearance. External wheels have a considerable impact on the overall aerodynamic performance of a racing car contributing about 35 per cent of the total vehicle drag force (Wright, 2004). Racing car teams are interested in understanding wheel aerodynamics since their complex wake structure influences the performance of the whole vehicle. At present, the wake structure of a wheel is not sufficiently well understood.

The majority of wind tunnel rolling roads do not allow the testing of a pneumatic tyre deformed by the application of a vertical load. This is mainly due to issues with repeatability and longevity of deformable tyres and also the possibility of catastrophic failure, especially with pneumatic tyres. Successfully replicating the deformation of a tyre at model-scale is difficult and requires the application of a large load, relative to the weight of the wheel, onto the moving ground belt, increasing belt wear. The use of non-deformable tyres, however, results in incorrect contact patch and tyre shoulder geometries. The pneumatic tyre used by Mears et al (2002a) was run at sufficiently high pressure as to be essentially solid. A solid tyre contact patch is reduced to a line and the upper and lower shoulders are identical due to the requirement for rotational symmetry. This also means that a cambered tyre profile has to be represented by a conical wheel when using a solid, axisymmetric tyre. The effect of camber on the wake of a non-deformable wheel is discussed by Knowles et al (2002). Purvis (2003), using a 50 per cent scale tyre, constructed from polyurethane foam, made total pressure measurements in

planes perpendicular to the freestream with varying degrees of tyre deformation. The width of the wake was found to increase as contact patch size (tyre deformation) was increased. At the present time wind tunnel testing with deformable wheels remains uncommon.

Experimental studies to determine wheel forces have relied on two techniques: direct force measurement using a wind tunnel balance or load cell; forces derived from the integration of surface static pressures. Both techniques have proved difficult to implement. Morelli (1969) overcame some of the problems by allowing the rotating wheel to protrude through the ground plane, thereby ensuring that no physical contact was made and recorded a net downforce ($C_L \approx -0.075$) on the wheel. This was contradicted by Stapleford and Carr (1970) ($C_L \approx 0.4$) and Cogotti (1983) ($C_L \approx 0.18$), using a similar experimental approach. Morelli's (1969) experimental set-up was flawed: the gap between the rotating wheel and the ground changed the pressure distribution around the wheel and gave rise to a wheel down-force. Stapleford and Carr (1970) and Cogotti (1983) sealed the gap with flexible materials giving a more realistic representation of the flow-field and therefore forces. Wäschle et al (2004), using a similar technique to that of Stapleford and Carr (1970) and Cogotti (1983), reported wheel forces in qualitative agreement with these early works. The pressure integration method of determining wheel forces is hindered by the need to measure static pressure on a rotating system. Fackrell (1974) and Fackrell and Harvey (1973, 1974) were the first successfully to apply the technique and published results which were in qualitative agreement with those of Stapleford and Carr (1970) and Cogotti (1983) ($C_L > 0$). More recently Hinson (1999), Skea et al (2000) and Mears (Mears and Dominy,

2004; Mears et al, 2002a,b, 2004) have made measurements using the pressure integration method. Quantitative comparisons are difficult due to the different wheel geometries used, however, the results do agree qualitatively.

Fackrell (1974) had successfully shown that rotation and ground motion were essential to simulate isolated wheel flows correctly. It remained for several subsequent studies to confirm that a moving floor and rotating wheels were essential for correct full-vehicle simulation. These included the work on road cars of Hackett et al (1987) at Ford, Bearman et al (1988) at Imperial College and Mercker and Berneburg (1992); Mercker et al (1991) with General Motors, and on racecars by Wildi (1994) and Mueller et al (1999) at Porsche.

Basara et al (2000), Axon (1999) and Skea et al (1998) were the first to publish the results of CFD studies of wheel flows, doing so in the late 1990s. Each study used a different commercial, finite-volume code based upon the use of structured grids and Reynolds-Averaged Navier-Stokes (RANS) equations. The effects of turbulence model and solver numerics were assessed in each case although no consensus was reached. Similar work has recently been carried out by Mears and Dominy (2004). Whilst the isolated wheel data produced by these studies did not add to those of Fackrell, they did show that CFD could be used to provide qualitative information about this type of flow-field. One particular cause for concern was the poor prediction of flow separation and lift and drag forces by all turbulence models and discretisation schemes. Wäschle et al (2004) showed that improved predictions of both the flow-field and lift-force were possible with a code based not upon RANS, but on the Lattice-Boltzmann method. In this work two

commercial codes were compared and the results validated using force, pressure and velocity data collected by the authors.

Fackrell (1974) measured total pressure in the wheel wake using a Kiel tube. The wake behind the rotating wheel was found to be taller than the stationary case but had a narrower ground lobe. Using Fackrell's wheel, Bearman et al (1988) made 9-hole probe measurements in a plane $2.5D$ downstream of a stationary wheel and one rotating on a moving ground. This showed the rotating-wheel wake to be dominated by a contra-rotating vortex pair centred approximately $0.25D$ above the ground (Figure 1) and higher than those behind the stationary wheel, which were centred just above the ground. This work confirmed, as far as was possible, Fackrell's 1974 conclusion that the vortices surrounding the stationary and rotating wheels were generated by different mechanisms. The multi-hole probe measurement technique was subsequently employed with success by Mears (Mears and Dominy, 2004; Mears et al, 2002a,b, 2004). The results of these investigations further clarified the structure of the wake downstream of an isolated wheel, concurring with the model proposed by Bearman et al (1988).

Cogotti and De Gregorio (2000) also applied the multi-hole probe technique to full-scale, housed-wheel flows, measuring the ground vortex at the exit of a wheel-arch. A single plane, perpendicular to the freestream, was investigated using particle image velocimetry (PIV) and laser Doppler anemometry (LDA) in addition to a multi-hole probe. All three techniques were found to be in good agreement. The work did not aim to investigate the flow, but prove that non-intrusive laser-based flow diagnostics can be applied to full-scale automotive testing.

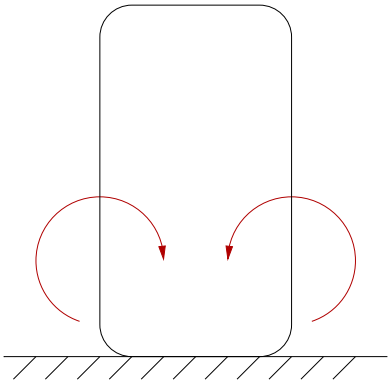

Figure 1 Schematic of vortex location and sense 2.5D downstream of wheel axis (after Bearman et al (1988)).

The most complete investigation of the velocities in the wake of an isolated wheel was carried out by Nigbur (1999). Three-dimensional velocities were measured using a hot-wire anemometer (HWA) in ten planes perpendicular to the wake of a 50 per cent-scale Formula One wheel. The data were presented as time-averaged contours for each velocity component along with contours of the associated root-mean-square (RMS) fluctuations. The in-plane (v-w) components were not combined into vectors making it impossible to analyse the vortical structures in the wake, however, the streamwise (u) data were more informative, exhibiting the lobed shape measured by Fackrell (1974) and showing regions of high turbulence intensity, particularly in the wake of the support strut. Unfortunately, the HWA was insensitive to the direction of the streamwise component and therefore no regions of reversed flow were identified. Also, the moving ground plane was approximately the same size as the wheel and therefore could not suppress fully the ground plane boundary layer growth. It was presumed that this was the cause of the strong asymmetry noted in the wake.

Wäschle et al (2004) made LDA measurements in the wake of a stationary and a rotating slick Formula One wheel in two measurement planes approximately $0.7D$ and $1.9D$ downstream of the wheel axis. Reversed flow regions were identified at the $0.7D$ measurement plane, however, the ground lobes reported by previous authors were poorly captured. This may be due to the apparently low resolution of the measurements.

Figure 2 presents two independent models of the structure of the flow downstream of an isolated wheel rotating in ground contact. Each arrow on the figure represents the projection of a streamwise trailing vortex and illustrates its size and rotational sense. Both models were proposed from consideration of vortex theory and not from measurements of velocity in the near-wake. It was proposed that:

- the upper vortices are conventional trailing vortices as associated with lifting bodies;
- the middle or hub vortices are formed by flow leaving the hub with rotation along the wheel axis and being turned by the main flow to a stream-wise orientation;
- the lower vortices originate from the strong viscous actions in front of the tyre contact patch; these vortices were termed “jetting vortices” by Mercker and Berneburg (1992).

Neither of these wake models has been demonstrated to exist, either through experimental measurements or numerical simulation. Notwithstanding the fact that the theoretical model in Figure 2(a) is unsubstantiated by the subsequent experimental work of Bearman et al (1988) and that there is a lack of velocity data to support Figure 2(b), both models have been accepted and re-published in respected

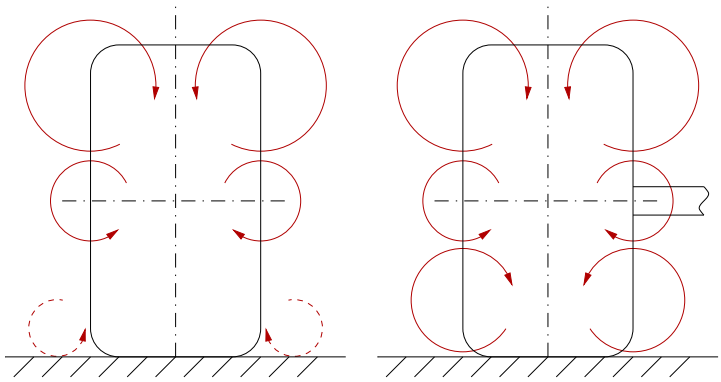

(a) After Cogotti (1983).

(b) After Mercker and Berneburg (1992).

Figure 2 Models of the trailing vortex system induced by a wheel rotating on the ground.

reference works. Cogotti (1983) appears in Racecar Vehicle Dynamics (Milliken and Milliken, 1995), and Mercker and Berneburg (1992) in Aerodynamics of Road Vehicles (Hucho, 1998).

The present paper presents new experimental data on the near wake of an isolated Formula One racing car wheel rotating in contact with the ground and, based on these measurements, proposes a new model of the trailing vortex system.

2 Aims and objectives

The aim of this study was to identify the prominent features of the wake of an isolated Formula One wheel rotating in ground contact and clarify the disparate models presented in the literature to date. The main objective of the tests was to extract three-dimensional mean velocity data from the near-wake of the wheel.

For the purposes of this study, the term near-wake will refer to the region less than one wheel diameter downstream of the wheel axis.

3 Experimental set-up

The experimental set-up consisted of three main parts, the wind tunnel, the test components and the LDA. These are described in more detail in the following subsections.

3.1 Wind Tunnel

A 2.74 m by 1.66 m closed-return, three-quarter open-jet wind tunnel (Figure 3) was used for all testing. A continuous-belt rolling road system, which was synchronised with the tunnel freestream velocity, provided both ground simulation and wheel rotation. Suction was applied through the floor immediately after the nozzle exit to remove the tunnel boundary layer. A-priori optimisation of the level and distribution of the suction, coupled with knife-edge transition to the belt, ensured minimal belt boundary layer. A vertical profile of total pressure normalized with the tunnel centreline value is shown in Figure 4. There is a small total pressure gradient giving an approximately 0.7 per cent increase as the belt is approached. The minimum recorded total pressure was 99.76 per cent of the freestream value at 0.754 mm above the belt surface. Distributed suction was also applied to the underside of the rolling-road belt to eliminate any belt lifting caused by aerodynamic loading and/or belt expansion. Air and road temperatures were held constant ($25 \pm 0.5°C$) throughout testing by individual chiller units. Further details of the wind tunnel, rolling road and calibration are given in Finnis et al (2000).

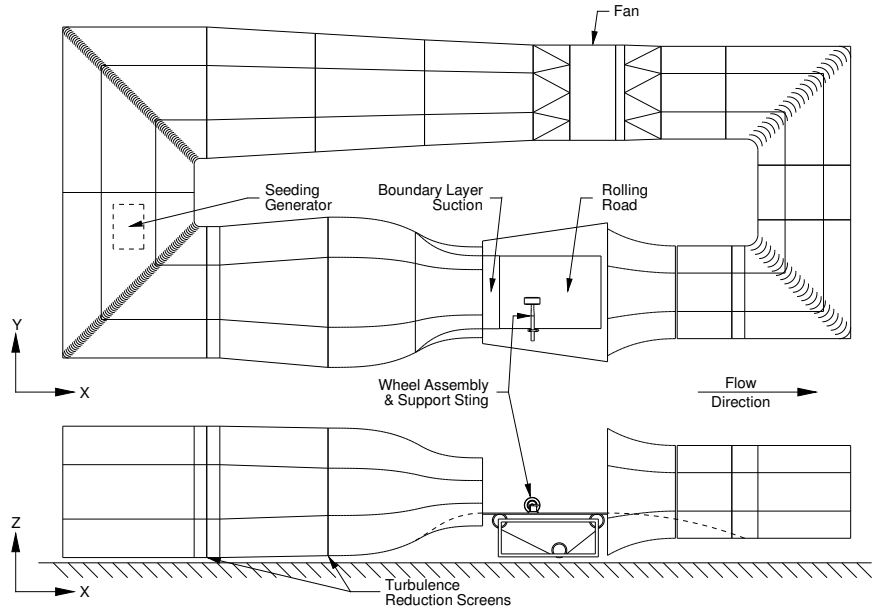

Figure 3 Schematic representation of the experimental set-up.

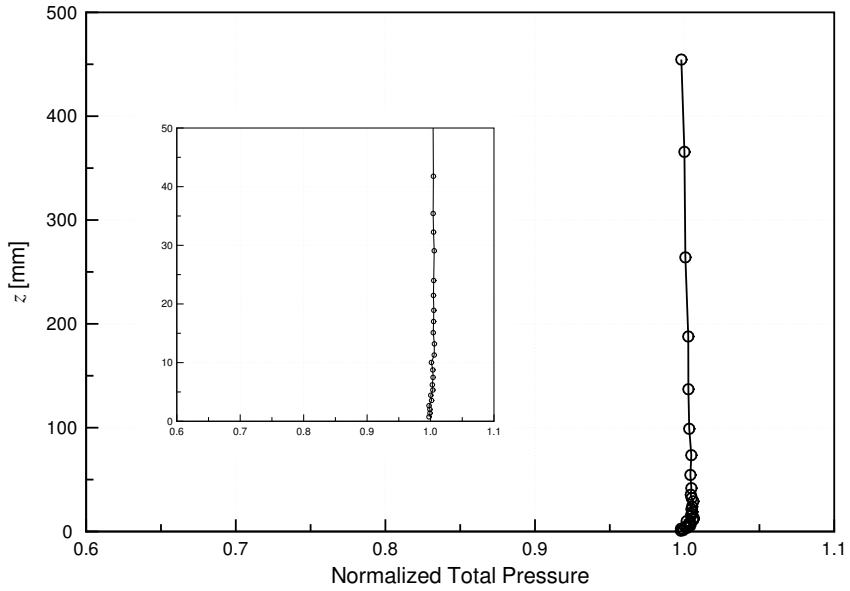

Figure 4 Boundary layer profile at the wheel test location.

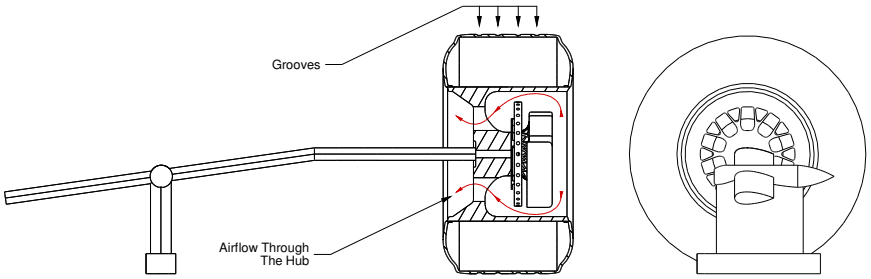

Figure 5 Formula One wheel assembly and support sting.

3.2 Test components

3.2.1 Wheel and sting assembly

The 50 per cent-scale Formula One front wheel assembly is shown cross-sectioned in Figure 5 together with the support sting. All of the components were in active service in racing car aerodynamic development when tested and as such represented the state-of-the-art in wind tunnel equipment.

The model-scale hub was machined from aluminium and featured two ultra-low-friction bearing units upon which it rotated. The hub was a detailed scale replica of that used on the actual racing car including the intricate spoke pattern. A non-deformable, carbon-fibre tyre with a lacquered surface finish was mounted on the hub. The wheel assembly was completed by a ventilated brake rotor and a suspension upright, both equally as detailed as the hub. The brake was mounted directly on the hub and as such rotated with it acting as a centrifugal pump. The upright was held stationary by mounting it on the support strut assembly. Both components provided a blockage to flow through the spokes and also partially

filled the deep cavity of the hub making the isolated wheel assembly geometrically similar to the conventional configuration mounted on a racing car.

The sting (see Figures 5 and 3.2.2) was mounted immediately beside the rolling road in a position similar to that in which it would sit if a full car were tested (see Figure 3). The sting has a symmetrical aerofoil cross-section with a thickness-to-chord ratio of 0.39. The reaction force between the belt and wheel was that due to the weight of the components. The sting applied no additional force to the wheel and routine checks with a stroboscope and optical tachometer showed there were no problems with wheel vibration or slipping during testing.

3.2.2 Laser doppler anemometer

The three-component LDA used in this study was a Dantec FibreFlow system operating in back-scatter mode. In order for the probes to remain outside the wind-tunnel jet, and maximise the non-intrusive quality of the LDA measurements, a long focal length ($f > 2$ m) was required. The LDA can operate at this distance, but only one $f = 2.5$ m lens was available and therefore only one probe could be used, limiting the simultaneous recording of velocity to two components; in practice, the quality of data was improved by measuring the components individually. Three tests, therefore, were needed for each measurement plane with a single velocity component recorded in each test. The resulting components were then combined and transformed into the wind-tunnel frame of reference.The fibre-optic beam delivery system included a Bragg cell to frequency shift one of the beam pairs by 40 MHz and allow resolution of flow direction as well as magnitude. The probe was rigidly mounted to a computer-controlled, three-component

traverse whose axes were set up parallel to those of the wind tunnel. The signal from the beam pair was processed by a burst spectrum analyser (BSA) and controlled by Dantec BSA Flow software v.1.4. The surfaces of the road and wheel were found to reflect the laser light back towards the probe reducing the signal-to-noise ratio. The reflections from the road did not significantly affect the quality of the data and the region affected by the wheel was limited to approximately 20 points in one traverse plane ($0.6D$ downstream).

Flow seeding was provided by a JEM Hot2000 fog generator producing high volume, ambient temperature seeding, with a mean particle size of 1.3 μm from a fluid which was 85 per cent water, 15 per cent ethylene glycol. The generator ran continuously throughout the tests, positioned inside the wind tunnel duct. It was found that with the seeder in the position indicated in Figure 3 the presence of a set of cascades and the turbulence-reduction screens rendered the seeder wake undetectable in the tunnel working section. Seeding density was adequate at all times although it reduced with time due to deposition on the screens, which were routinely cleaned to avoid further degradation of seeding density and flow quality.

3.3 Test procedure

Testing was carried out in the open jet wind-tunnel shown in Figure 3 at a freestream velocity of 30 ms^{-1}. This gave a Reynolds number, based on wheel diameter, of $6.8 \cdot 10^5$. All tests were carried out at constant velocity with the wheel in motion and as such did not address Reynolds number effects nor the relative effect of rotation, owing to the lack of a stationary datum case. The blockage, based

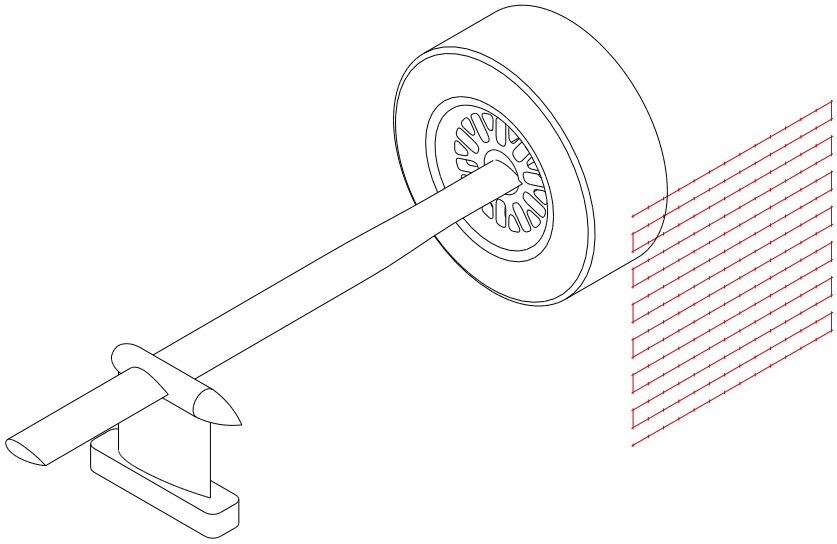

Figure 6 Example measurement plane.

on the ratio of projected frontal areas of the wheel and wind-tunnel nozzle was 1.4 per cent. The mean freestream turbulence intensity was 0.25 per cent.

613 data points were arranged in a $y-z$ planar grid with dimensions of 0.34 m by 0.34 m, perpendicular to the freestream (Figure 6). The spatial resolution of the measurement plane (20 mm and 10 mm in the y- and z-directions respectively) was dictated by the size of the LDA measurement volume and was chosen to ensure that the measurement volume at each point was unique and did not overlap that of other points. The measurement plane, centred about the wheel centreline, was positioned at three streamwise locations from the wheel axis; $0.6D$, $0.75D$ and $1D$.

It was not possible to predetermine the time taken to gather the data due to the stochastic nature of LDA sampling. In all tests, and for all measurement

points, the maximum sampling time (20 seconds) and maximum number of samples (5000) remained constant; reaching either target would trigger movement to the next point. This was an attempt to maximise the sample population without an excessive acquisition time. A five second pause was inserted after each movement of the traverse in order to allow any induced probe vibration to decay.

4 Error analysis

A breakdown of the experimental errors and their determination is given below.

4.1 Velocity

The wind tunnel control system was able to maintain the freestream air velocity to within ± 0.06 ms^{-1} and the rolling road belt speed to within ± 0.02 ms^{-1}.

4.2 Measurement location uncertainty

The size of the LDA measurement volume introduced a systematic error in the measurement location. Velocity could be recorded from anywhere within that volume and therefore the maximum location error was one half of the volume's dimensions. The resultant errors have been transformed into the tunnel frame of reference to account for the orientation of the probe and were determined to be ± 4.1 mm in the x-axis, ± 5.5 mm in the y-axis and ± 1.5 mm in the z-axis.

4.3 Seeding response

The seeding system provided a large volume of uniform-diameter (1.3 μm), ambient-temperature seeding particles. The error introduced by the inability of the seeding to follow the flow was assessed using the method of Dring (1982) in which the response of a particle to an acceleration of the surrounding fluid is related to its Stokes number (estimated here to be $6.4 \cdot 10^{-4}$). For Stokes numbers less than 0.01, the maximum velocity error is equal to the Stokes number (Dring, 1982) and therefore the error due to the response of the seeding was negligible.

4.4 Velocity bias

At a given point in a uniformly-seeded flow a velocity fluctuation above the mean value would carry more particles through the measurement volume generating more samples than a similar fluctuation below the mean. In this way the mean velocity calculated from the raw samples will be biased towards the higher velocities. The velocity bias was removed by weighting the samples by a factor inversely proportional to the velocity of the sample during calculation of the mean value. The particle transit time (the time taken for the particle to cross the measurement volume), t, was used as the weighting factor (Buchave et al, 1979).

4.5 Sampling error

The rate at which samples of a process are acquired has an impact on the uncertainty of the subsequently-calculated statistics, such as the population mean and variance. Since LDA samples are acquired when a particle crosses the mea-

surement volume, collection of statistically-independent samples is difficult. In Section 3.3 it was stated that the maximum number of samples and the maximum time spent at each measurement point were prescribed; the probe moved to its next location when one of these criteria was satisfied. The sampling rate varied with the measurement point and, therefore, so did the associated uncertainty. This uncertainty was estimated using the method of Benedict and Gould (1996) with the required integral timescale, τ_i, estimated using the method of Nobach (2000). Based on these techniques it was determined that, to a 95 per cent confidence level, 30 per cent of the measurement points had an error of less than 1 per cent and 70 per cent of the measurement points had an error less than 10 per cent.

5 Results and discussion

The experimental data in the three $y-z$ measurement planes are presented and discussed. These data provide clearer insight into the isolated wheel wake structure leading to a new wake model being presented for the present wheel geometry. In all cases the velocity and distance data were non-dimensionalized by the freestream velocity, u_∞, and the wheel diameter, D, respectively.

5.1 Mean streamwise velocity

Figure 7(a) shows that the near wake is made up of a central region, with approximately the same dimensions as the projected wheel profile, accompanied by two large ground lobes. The central region and ground lobes form a wake whose shape is similar to an inverted-T ($\perp$). The features (particularly the ground lobes) are not symmetrical about the $y = 0$ plane due to the influence of the support sting, whose

wake is clearly visible in each of the measurement planes. The general shape of the wake is in agreement with the previous experimental works of Fackrell (1974), Nigbur (1999) and Purvis (2003), although the measurement techniques used in those studies did not allow the identification of reversed flow. The existence of recirculation zones was expected, following consideration of the recirculation zones prevalent in bluff-body wakes; the extension of this region outside the projected profile of the wheel is, however, more unusual. The data provide significantly more detail than those presented by Wäschle et al (2004), which did not identify the ground lobes at $x/D < 1$.

Further investigation, combined with the use of numerical techniques (Knowles, 2005) provided an explanation for the reversed flow regions extending beyond the projected profile of the wheel. It is proposed that, just upstream of the contact patch, the convergence of the tyre and road surfaces produces a localised lateral jet on each side of the wheel. The jets deflect the freestream flow as it passes the lower shoulders of the wheel, thus modifying the wheel's effective shape. It is this deflection that generates the lower lobes, which cause the observed regions of reversed flow to extend beyond the projected profile of the wheel.

5.2 In-plane ($v - w$) velocity data

The asymmetry noted in the u-velocity contours (Figure 7(a)) is also visible in the velocity vector plots of Figure 7(b) and also in Figure 7(c), which presents the measured in-plane velocity data using the line integral convolution (LIC) technique (Knowles et al, 2006). LIC images offer greatly improved visualization of

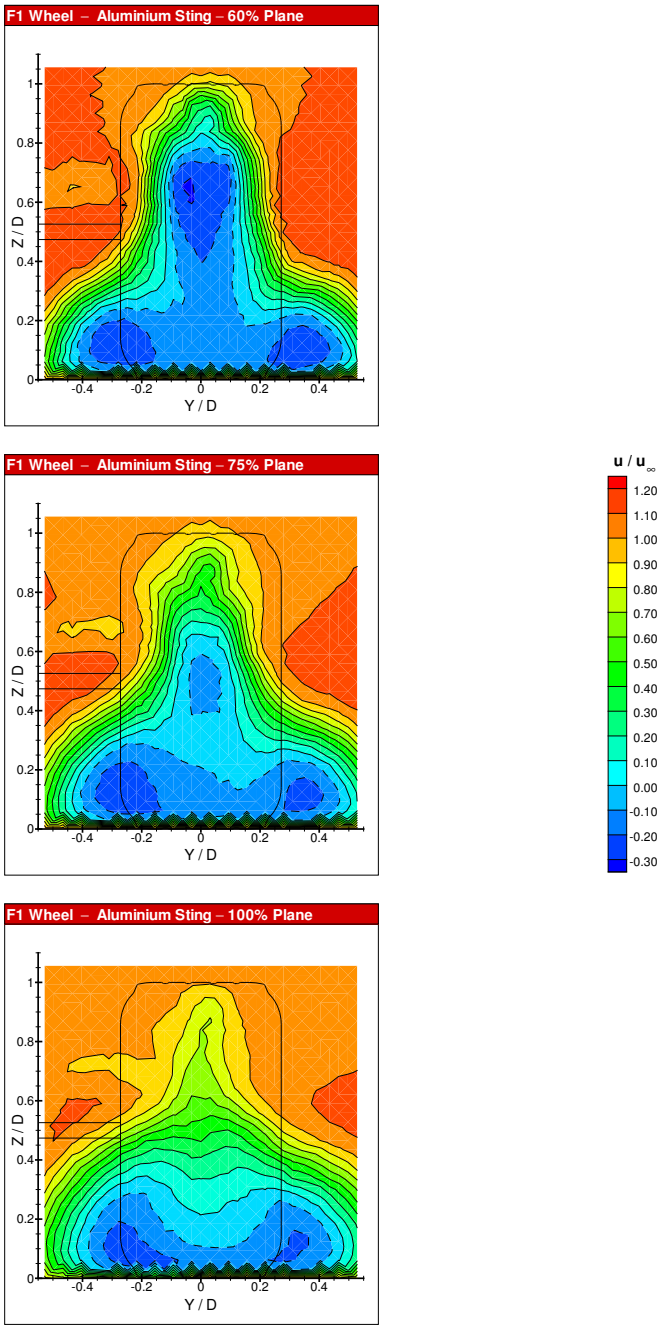

(a) Contours of mean u velocity (negative regions bounded by dashed lines).

Figure 7 Isolated Formula One wheel data for $x/D = 0.6$, 0.75 and 1.0 respectively.

planar flow features at the expense of the magnitude and direction information provided by velocity vectors.

In the measurement plane closest to the wheel ($0.6D$ downstream) four vortical regions were observed to be present; two upper vortices and two lower ones. The left and right vortices were separated by a strong central down-wash region. The vortex centres remained within, or aligned with, the projected profile of the wheel and were accompanied by large regions of up-wash on either side of the wheel. This up-wash explains why the wake of the sting in Figure 7(a) is observed to convect upwards in each successive downstream plane.

In an attempt to clarify the origins of the upper trailing vortices further measurements were made in a plane located $0.4D$ downstream of the wheel axis. This plane intersects the tyre which, coupled with points lost due to reflections from the tyre and hub surface, dictated that only the 127 uppermost points could be investigated. These points were processed using the LIC technique and the results are shown in Figure 8. This confirms that the upper vortices have their origins at the top of the wheel. Their position inside the projected profile of the wheel suggests that they roll up from the shoulders of the tyre immediately upstream of the flow separation.

The upper vortices are convected downwards quite quickly by the strong central down-wash region and at the $0.75D$ measurement plane appear to have merged with the two lower vortices. At $1D$ downstream, no evidence of the upper vortices remains and the flow is dominated by the lower vortices, which have grown in size.

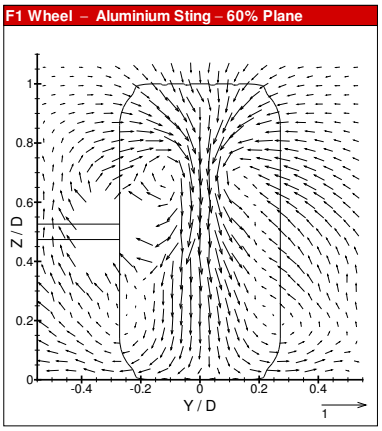

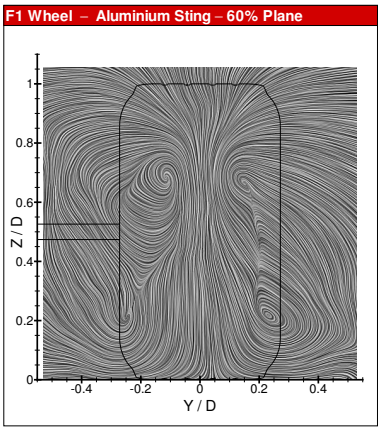

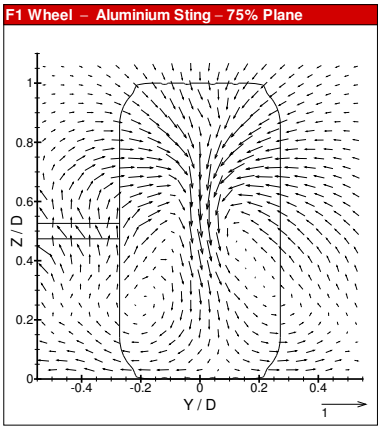

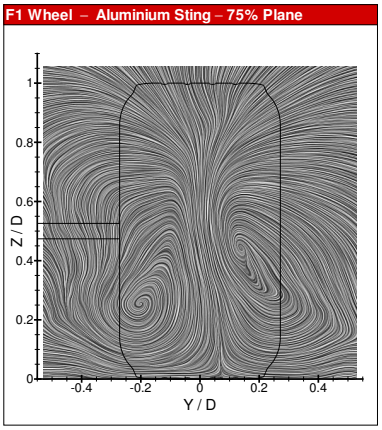

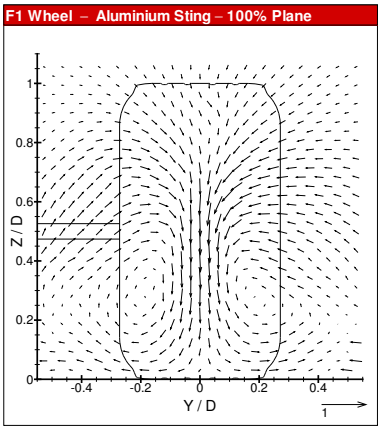

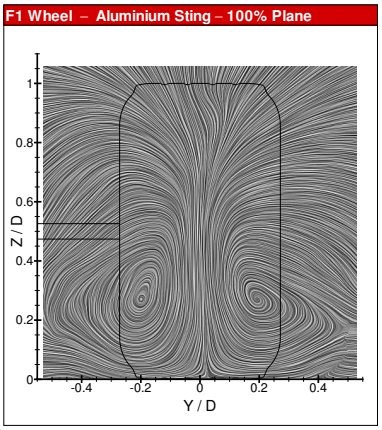

(b) In-plane ($v-w$) velocity vectors. (c) Line integral convolution images.

Figure 7 Isolated Formula One wheel data (continued).

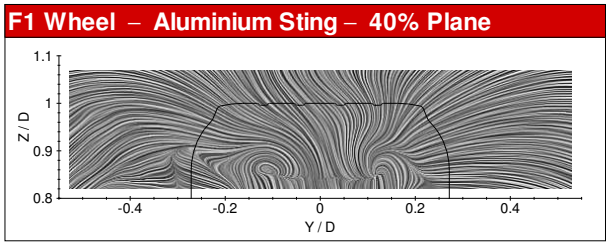

Figure 8 Isolated Formula One wheel data – identification of upper vortices at $x/D = 0.4$.

5.3 Wheel wake structure

In the light of the experimental measurements described in Sections 5.1 and 5.2 above, the two models of the trailing vortex structure of an isolated wheel rotating in ground contact (Figure 2) were revisited. The hub vortices, described in the literature, were not observed experimentally for the present hub geometry (which had a brake-induced outflow), neither were they identified in similar research on a Champ Car wheel (which had a brake-induced inflow; Knowles et al (2002)). It is proposed that any hub flow is quickly swept up into the upper and lower vortices. The lower vortices were larger and more clearly defined than the upper vortices, which appeared to merge with the lower vortices within $1D$ downstream of the wheel axis. This would explain the presence of just two trailing vortices as observed by Bearman et al (1988) since in that case measurements were made $2.5D$ downstream of the wheel axis.

As a consequence of these findings a new model of the trailing vortex system is presented in Figure 9. The model is intended to represent a generic wheel and as such does not include any asymmetries, which were present in the current experimental results and thought to be caused by the presence of the support sting.

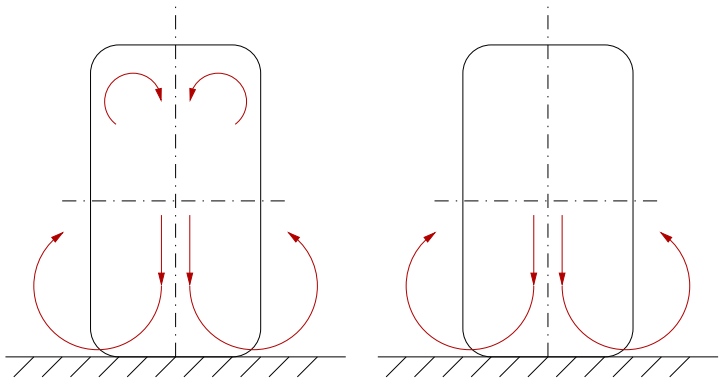

(a) $x/D < 1$. (b) $x/D \geq 1$.

Figure 9 Proposed model of the trailing vortex system of an isolated wheel rotating in ground contact.

6 Conclusions

An experimental investigation was conducted with the aim of clarifying the structure of the near-wake of an isolated Formula One wheel rotating in ground contact. The following features were identified as the main characteristics of such a wake.

- A region of velocity deficit in the shape of an inverted-T ($\perp$).
- Large regions of reversed flow existed in the wake. Near the ground, the region of reversed flow extends beyond the projected profile of the wheel.
- A trailing vortex system consisting of two contra-rotating vortex pairs, one in the upper half of the wake, and one at ground level.
- All four vortices are centred within, or aligned with, the projected profile of the wheel, have a streamwise axis and do not spread laterally up to one wheel diameter downstream.
- The ground vortex pair are larger and more defined than the upper vortices.

– The upper vortex pair merged with the ground vortex pair within one diameter downstream of the wheel's axis.

Acknowledgements Financial support from an Engineering and Physical Sciences Research Council CASE award and the loan of wind tunnel model components from Jaguar Racing is gratefully acknowledged.

References

Axon L (1999) The aerodynamic characteristics of automobile wheels – CFD prediction and wind tunnel experiment. PhD thesis, Cranfield University, Bedfordshire, UK

Basara B, Beader D, Przulj VP (2000) Numerical simulation of the air flow around a rotating wheel. In: 3rd MIRA International Conference on Vehicle Aerodynamics, Rugby, UK

Bearman PW, De Beer D, Hamidy E, Harvey JK (1988) The effect of a moving floor on wind-tunnel simulation of road vehicles. Technical Paper 880245, Society of Automotive Engineers, Warrendale, PA

Benedict LH, Gould RD (1996) Towards better uncertainty estimates for turbulence statistics. Experiments in Fluids 22(2):129–136

Buchave P, George Jr WK, Lumley JL (1979) The measurement of turbulence with the laser-doppler anemometer. Annual Review of Fluid Mechanics 11:443–503

Cogotti A (1983) Aerodynamic characteristics of car wheels. Int J of Vehicle Design, *Technological Advances in Vehicle Design Series, SP3*, Impact of Aerodynamics on Vehicle Design pp 173–196

Cogotti A, De Gregorio F (2000) Presentation of flow field investigation by PIV on a full-scale car in the Pininfarina wind tunnel. Technical Paper 2000-01-0870, Society of Automotive Engineers, Warrendale, PA

Dring RP (1982) Sizing criteria for laser anemometry particles. ASME Journal of Fluids Engineering 104:15–17

Fackrell JE (1974) The aerodynamics of an isolated wheel rotating in contact with the ground. PhD thesis, University of London, UK

Fackrell JE, Harvey JK (1973) The flow field and pressure distribution of an isolated road wheel. In: Stephens HS (ed) Advances in Road Vehicle Aerodynamics, BHRA Fluids Engineering, Cranfield, UK, pp 155–165

Fackrell JE, Harvey JK (1974) The aerodynamics of an isolated road wheel. In: Pershing B (ed) 2nd AIAA Symposium of Aerodynamics of Sports and Competition Automobiles, Western Periodicals Co., Los Angeles, CA, vol 16, pp 119–125, iSBN 0879380284

Finnis MV, Knowles K, Lewis R, Pitchforth D, Reynard AJ (2000) A new 3/4 open-jet wind tunnel for racing car aerodynamic testing. In: 3rd MIRA International Conference on Vehicle Aerodynamics, Rugby, UK

Hackett JE, Baker JB, Williams JE, Wallis SB (1987) On the influence of ground movement and wheel rotation in tests on modern car shapes. Technical Paper 870245, Society of Automotive Engineers, Warrendale, PA

Hinson M (1999) Measurement of the lift produced by an isolated, rotating formula one wheel using a new pressure measurement system. MSc thesis, Cranfield University, Bedfordshire, UK

Hucho WH (ed) (1998) Aerodynamics of Road Vehicles, 4th edn. Society of Automotive Engineers, Warrendale, PA

Knowles R, Saddington A, Knowles K (2002) On the near wake of rotating, 40%-scale Champ Car wheels. SAE 2002 Transactions - Journal of Passenger Cars: Mechanical Systems 6:2245–2253

Knowles RD (2005) Monoposto racecar wheel aerodynamics: Investigation of near-wake structure & support sting interference. PhD thesis, Cranfield University, Shrivenham, UK

Knowles RD, Finnis MV, Saddington AJ, Knowles K (2006) Planar visualization of vortical flows. IMechE Part G: Journal of Aerospace Engineering 220(6)

Mears AP, Dominy RG (2004) Racing car wheel aerodynamics – Comparisons between experimental and CFD derived flow-field data. Technical Paper 2004-01-3555, Society of Automotive Engineers, Warrendale, PA

Mears AP, Dominy RG, Sims-Williams DB (2002a) The air flow about an exposed racing wheel. Technical Paper 2002-01-3290, Society of Automotive Engineers, Warrendale, PA

Mears AP, Dominy RG, Sims-Williams DB (2002b) The flow about an isolated rotating wheel – Effects of yaw on lift, drag and flow structure. In: Proceedings of the 4th MIRA International Vehicle Aerodynamics Conference, Warwick, UK

Mears AP, Crossland SC, Dominy RG (2004) An investigation into the flow-field about an exposed racing wheel. Technical Paper 2004-01-0446, Society of Automotive Engineers, Warrendale, PA

Mercker E, Berneburg H (1992) On the simulation of road driving of a passenger car in a wind tunnel using a moving belt and rotating wheels. In: Proceedings of 3rd International Conference on Innovation and Reliability, Florence, Italy

Mercker E, Breuer N, Berneburg H, Emmelmann HJ (1991) On the aerodynamic interference due to the rotating wheels of passenger cars. Technical Paper 910311, Society of Automotive Engineers, Warrendale, PA

Milliken WF, Milliken DL (1995) Racecar Vehicle Dynamics. Society of Automotive Engineers, Warrendale, PA

Morelli A (1969) Aerodynamics actions on an automobile wheel. In: 1st Symposium on Road Vehicle Aerodynamics, City University, London, Paper 5

Mueller R, Singer N, Eckert W (1999) Moving belt with distributed suction in the Porsche model wind tunnel. Technical Paper 1999-01-0650, Society of Automotive Engineers, Warrendale, PA

Nigbur JE (1999) Characteristics of the wake downstream of an isolated automotive wheel. MSc thesis, Cranfield University, Bedfordshire, UK

Nobach H (2000) A global concept of autocorrelation and power spectral density estimation from LDA data sets. In: 10th International Symposium on Applications of Laser Techniques to Fluid Mechanics, Instituto Superior Técnico, Lisbon, Portugal

Purvis AR (2003) The wake behind a deformable racing tyre. MSc thesis, Cranfield University

Skea AF, Bullen PR, Qiao J (1998) The use of CFD to predict the air flow around a rotating wheel. In: 2nd MIRA International Conference on Vehicle Aerodynamics, Birmingham, UK

Skea AF, Bullen PR, Qiao J (2000) CFD simulations and experimental measurements of the flow over a rotating wheel in a wheel arch. Technical Paper 2000-01-0487, Society of Automotive Engineers, Warrendale, PA

Stapleford WR, Carr GW (1970) Aerodynamic characteristics of exposed rotating wheels. Report 1970/2, Motor Industry Research Association, Nuneaton, UK

Wäschle A, Cyr S, Kuthada T, Wiedermann J (2004) Flow around an isolated wheel – experimental and numerical comparison of two CFD codes. Technical Paper 2004-01-0445, Society of Automotive Engineers, Warrendale, PA

Wildi J (1994) Wind tunnel testing of racing cars – the importance of the road simulation technique. In: Royal Aeronautical Society Conference on Wind Tunnels and Wind Tunnel Testing, Loughborough, UK

Wright PG (2004) Ferrari Formula 1: Under the Skin of the Championship-Winning F1-2000. Society of Automotive Engineers, Warrendale, PA